R. & M. No. 3292

MINISTRY OF AVIATION

AERONAUTICAL RESEARCH COUNCIL
REPORTS AND MEMORANDA

Further Results on the Mixing of Free Axially-Symmetrical Jets of Mach Number 1·40

By N. H. JOHANNESEN

DEPARTMENT OF THE MECHANICS OF FLUIDS, UNIVERSITY OF MANCHESTER

LONDON: HER MAJESTY'S STATIONERY OFFICE

1962

ELEVEN SHILLINGS NET

Further Results on the Mixing of Free Axially-Symmetrical Jets of Mach Number 1·40

By N. H. JOHANNESEN

DEPARTMENT OF THE MECHANICS OF FLUIDS, UNIVERSITY OF MANCHESTER

*Reports and Memoranda No. 3292**
May, 1959

Summary. An axially-symmetrical supersonic fully-expanded jet of diameter 0·75 in. was investigated by pitot- and static-tube traverses in the region from the exit to 100 diameters downstream. The investigation is supplementary to that reported by Johannesen[3]. In the jet discussed in this report the initial internal disturbances were weak, as compared with those in the jet investigated previously. The structures of the mixing regions in the initial parts of the two jets showed substantial differences. Further downstream the jet with weak internal disturbances showed a very slow approach to self-preserving flow. This was clear from the curves of the jet width and of the reciprocal of the centreline velocity plotted against distance from the exit approaching straight lines only slowly, but was particularly clearly indicated by the static-pressure distributions. The ratio of static pressure to dynamic pressure showed no tendency to become constant on the axis, even at the last station of measurement. The relation between the static-pressure distributions and the jet turbulence is discussed and it is shown that if the classical corrections to the readings of pitot and static tubes are adequate the errors in the deduced structure of the jet, ignoring these corrections, may be very considerable.

1. *Introduction.* A previous report (Ref. 3) described experimental results on the mixing of axially-symmetrical jets of Mach number 1·40. The present report contains supplementary results and is a direct continuation of the previous report which will in what follows be referred to as 'Part I'. It will be assumed that the reader is familiar with Part I which contained full descriptions of the experimental equipment and technique.

Part I described the photographic investigations of the jets from a series of nozzles numbered 1 to 6, all of exit diameter approximately 0·75 in. and designed to give an exit Mach number of 1·40 at the design pressure ratio. The Appendix gives details of Nozzles 1 and 6. Jet 1 was the extreme case of a jet with strong internal shock waves, whereas in Jet 6 the internal disturbances appeared on the photographs to have been reduced to very weak ones. Part I also contained the results of the pressure traverses across Jet 1. The pitot traverses could only be carried out successfully for values of x, the distance from the nozzle exit, from 0 to 2·5 in., because at higher values of x unsteadiness of the flow made the readings uncertain and unrepeatable. Static traverses were not considered reliable because of the strong and unknown effects of the interaction between the static-tube boundary layer and the shock waves in the jet.

The main theme of the present report is the results of the pressure traverses carried out on Jet 6. In this jet no difficulties due to unsteadiness were encountered and it was therefore possible to

* Previously issued as A.R.C. 20,981.

extend the pitot traverses to large values of x. The highest value of x used, 70 in., was in fact determined by the limitations of the traversing gear. Also, the internal disturbances in Jet 6 were sufficiently weak for static-pressure traverses to be possible. These were therefore carried out for all values of x except very close to the nozzle exit.

The discussion of the pressure traverses of Jet 6 will be divided into two sections, one for the range of x from 0 to 2·5 in., the other for the range from 3·0 to 70·0 in. The first section covers the same range of x as the available results for Jet 1. This division is also convenient for another reason. The value of x of 3·0 in. roughly separates the region near the exit where a solid core remains in the jet from the downstream region of fully-developed jet flow.

2. *Pressure Traverses for x from 0 to 2·5 in.*

(*a*) *Survey of Traverses.* The jet from Nozzle 6 was traversed with the 1 mm outside diameter pitot tube in the horizontal plane of symmetry at the following values of x: 0, 0·1, 0·2, 0·3, 0·4, 0·5, 0·6, 0·8, 1·0, 1·5, 2·0 and 2·5 in. These values of x are the same as those for the traverses of Jet 1. Furthermore, Jet 6 was traversed with a 1 mm outside diameter static tube at the stations for $x \geqslant 0{\cdot}6$ in. Static traverses at smaller values of x were not possible because the nose of the static tube was then inside the exit plane of the nozzle and the tube could only be moved across the core of the jet.

As described in Part I, the non-dimensional pitot-pressure distributions were plotted against distance across the jet with an arbitrary zero and used to determine the axes of symmetry of the profiles. Some asymmetry was noted in some of the profiles and made the determination of the axis difficult. This asymmetry was more clearly observable in the velocity profiles and will be discussed in detail later.

The readings in the exit plane of the nozzle ($x = 0$) were treated as described in Part I.

(*b*) *Velocity Profiles.* It was discussed in Part I how the velocity profiles may be determined from the measured distributions of pitot and static pressures, assuming the stagnation temperature constant throughout the flow. For Jet 1 the static pressures were not measured and the static pressure was assumed to be equal to the barometric pressure throughout the mixing region. For Jet 6 static-pressure distributions were available for $x \geqslant 0{\cdot}6$ in. In order to investigate the effect of the small measured differences between static and barometric pressures in the mixing region, the velocity profiles in Jet 6 were, in the range of x from 0·6 to 2·5 in., at each value of x calculated both using the measured static pressure and using a constant value of the static pressure equal to the barometric pressure.

It was found that the difference between the two velocity profiles at each value of x was just detectable at $x = 2{\cdot}0$ and 2·5 in., but negligible at smaller values of x. This indicates that the errors in the velocity profiles for Jet 1 due to incorrect static pressure are likely to be small. For Jet 6 the profiles based on the measured static-pressure distributions were of course used for the following discussion.

The non-dimensional velocity profiles for Jet 6 in the region $x = 0{\cdot}6$ in. to $x = 2{\cdot}5$ in. are given in Figs. 14 to 19 which also contain the static-pressure distributions. These will be discussed later in connection with the discussion of the pressure distributions in the fully-developed jet.

(*c*) *Asymmetry of Profiles and Rate of Spreading.* When the velocity profiles at each value of x were plotted with arbitrary zero in order to check the determination of the axis of symmetry based on the pressure curves, the asymmetry already mentioned was quite noticeable. However, the

mixing-region width can be determined without a knowledge of the position of the axis. This was done using the three different definitions of the width, Δy_a, Δy_b, Δy_c (*see* Section 4c of Part I).

Because of the asymmetry it was necessary to distinguish between the Δy values on the two sides of each traverse. We shall call the two sides 'East' and 'West'. (The jet was traversed in the horizontal plane and the jet axis was pointing North.)

The East and West values of Δy_a, Δy_b and Δy_c in the range $0{\cdot}1$ in. $\leqslant x \leqslant 1{\cdot}0$ in. are shown on Figs. 1, 2 and 3. The differences between the East and West values are insignificant for the first three values of x but become quite pronounced for larger values of x. Also shown on Figs. 1 to 3 (as full lines) are the best straight lines for Jet 1 derived in Part I. We notice at once the apparent greater rate of spreading of the mixing region in Jet 6 than of the mixing region in Jet 1.

At this stage of the investigation two questions present themselves. Firstly, we ask: are the differences between the two sides of Jet 6 genuine and repeatable or are they simply due to experimental scatter? It must be remembered that we are discussing small differences in already small quantities. Secondly, we begin to wonder whether the assumptions on which the treatment of the measurements on Jet 1, as presented in Part I, were based, were justified. In the case of Jet 1 all the results presented in Part I were based on measurements in the East side of the jet, the measurements in the West side being used only to establish the apparent symmetry of the profiles and to determine the axis of symmetry. The results from Jet 6 make it look doubtful whether the assumption of axial symmetry is justified. Although the differences between the Δy values on the two sides are small, they seem to have a definite trend and, what is more important, there is no reason whatsoever to believe that we have found the minimum and maximum Δy values at each particular value of x. We have only traversed in one plane through the axis of the jet, and a complete investigation of the mixing region at any one value of x might well show much larger differences between the maximum and minimum Δy values.

In order to answer these questions, the measurements on Jet 1 were reconsidered and this time the Δy values were determined for both mixing regions at each value of x. The corresponding points are also shown on Figs. 1 to 3. It will be seen that the difference between the two sides of Jet 1 is much smaller than the corresponding difference for Jet 6. In fact, if we ignore our experience with Jet 6 it seems quite reasonable to use the results for one side of Jet 1 only and expect them to be representative of the jet. The full lines on Figs. 1 to 3 are the best lines through the East side points and are the same as those shown on Fig. 16 or Part I. They correspond to an average value of the scale factor σ of $21{\cdot}9$.

The calculation of σ for the region $0{\cdot}1$ in. $\leqslant x \leqslant 1{\cdot}0$ in. in Jet 1 (previously called Group I) was repeated using mean values of Δy for the two sides of the jet. The new value of σ was $22{\cdot}1$. This differs from the old value by an amount smaller than the expected experimental inaccuracy. The position of the virtual origin of the mixing region in the first inch of Jet 1 was also recalculated using both sides of the jet. The new value was found to be equal to the old value, $x = -0{\cdot}23$ in.

Next the question of the repeatability of the measurements on Jet 6 was investigated. The traverses at $x = 0{\cdot}5$ in. and $0{\cdot}6$ in. were repeated a number of times. The variations in Δy were found to be small in most cases but in a few cases the variation was as much as three quarters of the *difference* in Δy on the two sides. However, the general trend of Δy being greater on the West side than on the East side was never changed. We therefore conclude that there is a genuine difference between the two sides of Jet 6 and that the repeatability is not as good for this jet as it was for Jet 1.

During the check on the traverses in Jet 6 it was established that the measured profiles did not depend on the direction of traverse (whether it was from East to West or from West to East) or on the diameter of the pitot tube. (The *profile* does not depend on pitot-tube diameter, but there may be an overall displacement effect depending on pitot-tube diameter.)

For Jet 1 it was found that the mixing region could be divided into two groups with a change in σ from 21·9 to 11·9 and in virtual origin from $x = -0{\cdot}23$ in. to $x = +0{\cdot}31$ in., the change taking place in the neighbourhood of $x = 1{\cdot}0$ in. It has already been mentioned that recalculations of σ and the virtual origin gave good agreement with the old values for Group I ($x \leqslant 1{\cdot}0$ in.). The calculations were also repeated, using both sides, for Group II ($1{\cdot}0$ in. $\leqslant x \leqslant 2{\cdot}5$ in.). The new values were 11·7 for σ and $x = +0{\cdot}34$ in. for the virtual origin, again satisfactory agreement with the original values based on one side only.

Returning now to Jet 6, the results discussed so far for x up to 1·0 in. do not justify the drawing of straight lines through the Δy points. All results up to and including $x = 2{\cdot}5$ in. are shown on Figs. 4, 5 and 6 where the points are the means of East and West values. On these figures are also included as heavy lines the two straight lines used for Jet 1 (*cf.*, Figs. 16 and 17 of Part I). If for Jet 6 the mean values of Δy are used at each value of x it will be seen that the points are fairly well represented by single straight lines (shown dashed) extending all the way from $x = 0{\cdot}1$ in. to $x = 2{\cdot}5$ in. The scatter at small values of x appears rather insignificant when the points are plotted on this scale.

The best straight lines were calculated. The mean value of σ for all three graphs was found to be 13·7 and the position of the virtual origin was $x = +0{\cdot}03$ in. For Jet 6 it would not have been reasonable to try to fit the Δy values by two straight lines with a change in slope. Re-examination of Figs. 1 to 3 does show, however, that the rate of spreading is slightly smaller close to the origin than at larger values of x.

The pronounced and unexpected difference between the behaviour of the 'two-dimensional' parts of the mixing regions in the two jets indicates that parameters not usually considered in flows of the half-jet type must be important.

It is usually assumed that the flow will depend only on Mach number and Reynolds number. The Mach number was the same in the two jets and need not be considered any further. The Reynolds number is usually considered to be unimportant except very close to the exit. Even if it were important the difference between the Reynolds numbers, based for example on Δy_a, of the two jets at corresponding points is so small that one would not expect it to be significant.

We are therefore left with the basic assumption of the idea of dynamical similarity of the two systems, namely that the systems are geometrically similar. There are no solid boundaries in our problem, and the condition of geometrical similarity is therefore only violated by the fact that the two bounding 'uniform' streams are not strictly uniform, and that the deviations from uniformity are different in the two jets. That non-uniformities are present is obvious from the photographs which also show that they are different in the two jets. A detailed discussion of the differences seems pointless, as we do not know which types of non-uniformities have important effects on the mixing. A simple-minded approach to the problem would give the opposite result to that observed: one would have expected that the obviously stronger shock waves in Jet 1 would have caused greater irregularities of the flow and a higher turbulence level in the main stream and hence a higher turbulence level in the mixing region and a greater rate of spreading. This is not happening close to the origin, but is still believed to be the main reason for the difference in the behaviour of the jets far downstream.

(*d*) *Similarity of Profiles.* Following the method discussed in detail in Part I and using the position of the virtual origin and the value of σ found above, all the profiles were plotted non-dimensionally on two graphs, Fig. 7 for the East side and Fig. 8 for the West side. Also shown on these graphs are the functions F_1 and F_2 defined in Part I. We note that one graph corresponds to the whole range of x from 0·1 to 2·5 in. As was the case for Jet 1, the profiles show a high degree of similarity, in fact, the scatter is hardly greater than on Figs. 18 and 19 of Part I.

It would now have been possible to carry out the integrations across the mixing regions as for Jet 1. These integrations are, however, very lengthy and it seemed unlikely that the general results would have been significantly different from those found for Jet 1. Hence they were not carried out.

3. *Pressure Traverses for x from 3·0 to 70 in.*

(*a*) *Survey of Traverses.* Using the same pitot and static tubes as in the region close to the nozzle exit, the jet was traversed at the following values of x: 3, 4, 5, 6, 8, 10, 12, 14, 16, 18, 20, 22, 24, 28, 32, 36, 40, 50, 60 and 70 in. The radial distance between consecutive pressure readings increased from 1/26 in. (1 turn) at $x = 3·0$ in. to 20/26 in. (20 turns) at $x = 70$ in.

From $x = 3·0$ in. to $x = 18·0$ in. the pressures were read on mercury manometers and the velocities calculated as described in Section 2. For larger values of x water manometers were used, and in regions of the jet where the Mach number was less than 0·1 the velocities were calculated using Bernoulli's equation for incompressible flow.

The pressure distributions, in particular those of static pressure, will be discussed in detail later, but first we consider the velocity profiles.

(*b*) *Velocity Profiles.* In Section 2 the velocity profiles were made non-dimensional by dividing by the velocity at the inner edge of the mixing region, the core velocity, which was very nearly constant independent of x. For larger values of x the constant-velocity core disappears and the velocities are therefore related to the velocity U_1 on the axis of the jet.

Fig. 9 shows the non-dimensional velocity profiles for x equal to 0, 4, 8, 12, 16, 20, 24, 28, 32, 36, 40, 50, 60 and 70 in. The non-dimensional velocity profiles for the region $x = 3$ in. to $x = 8$ in. will be found on Figs. 20 to 24. In Fig. 9 the r-co-ordinate is in inches whereas in Figs. 20 to 24, r is made non-dimensional by division by $r_{0·5}$, the value of r at which $U/U_1 = \frac{1}{2}$.

(*c*) *Velocity on Axis and Spread of Jet.* The two parameters describing the overall development of the jet are the velocity on the axis, U_1, and some typical lateral dimension. The latter was chosen as $r_{0·5}$, the value of the radius at the point where $U/U_1 = \frac{1}{2}$. This was used rather than the value of r corresponding to some smaller value of the velocity ratio because of the increasing difficulties in measuring the velocity near the outer edge of the jet. These two parameters in non-dimensional form, U_1/U_i (and U_i/U_1) and $r_{0·5}/r_N$, are given in Fig. 10 as functions of the distance from the origin, x, in inches or non-dimensionally x/r_N. For comparison, the curve from Ref. 6 already given in Fig. 20 of Part I is again included. We notice that U_i/U_1 and $r_{0·5}/r_N$ are nearly constant up to $x/r_N = 14$ and then start increasing. The rates of increase with x eventually become very nearly constant.

(*d*) *Similarity of Profiles.* For fully self-preserving flow we would expect both $r_{0·5}$ and $1/U_1$ to increase linearly with x, measured from a suitable virtual origin, x_0. Both graphs on Fig. 10 suggest that x_0 is of order 15 to 20 r_N. It is, however, difficult to decide when the graphs become straight lines, the U curve approaching linearity rather more slowly than the r curve. It is also difficult to make the two asymptotes meet the axis in the same point. As will be clear from the discussion of the

static-pressure curves, the flow has not, in fact, reached a state of self-preservation even at the last station of measurement $x = 190r_N$. Any attempt to plot the velocity profiles against a non-dimensional co-ordinate $r/(x-x_0)$ on a single graph would therefore lead, at best, to a demonstration of approximate *fluid-dynamical* similarity. It was found that the profiles quickly approached *geometrical* similarity. This is demonstrated in Figs. 11 and 12. The profiles have been plotted on two graphs simply to avoid an over-crowding of points, not because there is any noticeable difference between the two sets of profiles. Also shown on Figs. 11 and 12 is the curve $U/U_1 = F_3 = \exp(-0{\cdot}6932(r/r_{0{\cdot}5})^3)$, in which the numerical factor is chosen to make the curve go through the points $r/r_{0{\cdot}5} = 1$, $U/U_1 = 0{\cdot}5$. The velocity profiles are well represented by this curve except near the outer edge.

(*e*) *Static-Pressure Field.* It has already been mentioned that the static-pressure distributions demonstrate that self-preservation has not been reached even at the largest values of x. The static-pressure traverses displayed many interesting features, and the implications cannot be fully appreciated until comparisons with experiments on other jets and, in particular, with measurements of turbulence, are possible. The author is not aware of any reports giving pressure distributions in comparable detail, and all the static-pressure distributions from Jet 6 are therefore included in the present report. Figs. 13 to 24 show the distributions $(P-B)/(H-P)_1$ for the region $x = 0{\cdot}0$ in. to $8{\cdot}0$ in. In Figs. 13 to 19 the radial co-ordinate is r/r_N and in the remainder of the figures it is $r/r_{0{\cdot}5}$. In Figs. 13 to 24 the non-dimensional velocity profiles are also included, as we shall find them useful in the interpretation of the pressure profiles. The slight asymmetry of the velocity profiles close to the exit makes an accurate determination of the axes of the profiles impossible but this is not important for the present discussion. The velocity profile in the plane of the exit has a discontinuity at the dotted lines. This is not genuine but caused by the fact that static-pressure measurements were only possible in the central region of the jet. Outside this region the velocity calculations were based on a static pressure assumed equal to atmospheric pressure.

In discussing Figs. 13 to 24 we may treat the pressure distributions in the mixing region and in the core separately. In the mixing regions we find a pressure defect associated with the turbulence (*see* below). The minimum is situated close to the point of inflection of the velocity profile. As the mixing region spreads into the core the pressure defect becomes more pronounced and the minima on the two sides move towards the axis where they eventually merge, and after $x = 8$ in. there is a single pressure minimum on the axis. This happens at a value of x about three times the value at which the two mixing profiles meet on the axis, indicating, it is believed, that a considerable distance is required for the centre region of the jet to become fully turbulent.

A close inspection shows that there is a tendency for the pressure in the mixing region to be lower on the right-hand side than on the left-hand side at least up to $x = 2$ in. The right-hand side corresponds to the West side, and we remember that this side was spreading more rapidly than the East side. There therefore seems to be a definite relationship between the rate of entrainment and the pressure defect. It should be emphasized that this relationship is not simply that the lower static pressure gives a higher velocity and hence a wider mixing region. It has already been mentioned that in the calculation of the velocity profiles the static-pressure defect is insignificant. The relationship is between pressure defect and lateral velocity.

In the core the flow is not turbulent, and some other explanation must be sought for the pressure variations. The standard explanation is, of course, that they are 'due to shock waves'. It is difficult, however, to see how a pressure field as that observed can be explained as the effect of a shock-wave

pattern. Ignoring for a moment the variations with r, we find that the general level of pressure varies with x. This variation is not inconsistent with the expected effect of shock and expansion waves being reflected from the edge of the jet. We see from Fig. 6 of Part I that weak waves are indeed present and that the full wavelength of the pattern is about $4r_N$ measured as the distance between two consecutive interactions of the same wave with the same side of the jet.

In addition to the variation of the general level of pressure with x there is a very persistent variation with r. At each value of x there is a maximum on the axis and two minima at r equal to $0{\cdot}2$ to $0{\cdot}3$ times r_N. No satisfactory explanation has been found for this pressure variation. It should be noted, however, that the variations in static pressure are very small compared with the dynamic pressure, and might therefore be caused by small interference effects, such as that of the bow wave from the tube being reflected from the mixing region.

Before we proceed to a discussion of the pressure profiles from $x = 10$ in. outwards we might consider the variation with x of the pressure defect on the axis. This is shown in Fig. 25. The non-dimensional pressure defect increases in the range of x from 10 to 28 in., reaching a peak value of order $0{\cdot}1$, and then falls off almost linearly with x. Measurements at larger values of x were not possible and it is therefore not known whether the non-dimensional pressure defect will level off to a constant final value.

The actual profiles are shown in Figs. 26 and 27. The graphs on Fig. 27 become more and more indeterminate as x is increased simply because of the limited sensitivity of the manometer.

It is interesting at this stage to compare our results with the few previously published results on the static-pressure distribution in free jets.

Warren[7] measured static-pressure profiles in axially-symmetric jets of Mach numbers $0{\cdot}97$ and $2{\cdot}60$ for values of x/r_N up to 60. The data given are not sufficiently detailed to allow a comparison with the results of the present report. The present author does not understand the discussion of the jet structure presented by Warren.

Pitkin and Glassman[5] studied a Mach number $2{\cdot}60$ axially-symmetric jet at sections spaced $10r_N$ up to $50r_N$. The results are similar to those presented in the present report but a detailed comparison is again difficult.

Miller and Comings[4] describe a detailed investigation of a two-dimensional low-speed jet in the region from the orifice to a distance of 40 times the orifice height. The investigation included static-pressure measurements and measurements of the mean velocity and the u-component of the turbulent velocity. Of particular interest to us are the static-pressure measurements. In the region close to the exit where a potential core was still present the static-pressure curves showed minima near the edge of the jet and a maximum (above atmospheric pressure) on the axis. At larger values of x the pressure curves had a single minimum on the centreline. The static-pressure defect on the centreline in terms of $\frac{1}{2}\rho U_1^2$ increased from $0{\cdot}030$ at x equal to 6 exit heights to $0{\cdot}116$ at x equal to 40 exit heights. This result seems to correspond to the region from 10 to 28 in. on our Fig. 25. The measurements were not extended to large enough values of x for the maximum of the curve to be reached.

(*g*) *Turbulence in the Jet and its Effect on the Pressure Readings.* The following discussion is limited to the case of incompressible flow. It will be found that the conclusions reached for the simpler case of constant density are such that attempting an extension to the case of compressible flow would be futile. It should be stressed that only a qualitative discussion is attempted. We shall throughout this section adopt a notation in which measured pressures and quantities derived from

them are written without suffix and the corresponding true (and unknown) quantities are indicated by the suffix t. The turbulent-velocity components have true values of u, v, w in cylindrical co-ordinates x, r, θ. The barometric pressure B is assumed known.

Examination of the orders of magnitude of the terms in the Reynolds equations of motion (*see* Ref. 6) shows that to a good approximation

$$B - P_t = \rho\overline{v^2}. \tag{1}$$

The only available expressions for the readings of pitot and static tubes in turbulent flow are those given by Goldstein[2] and Fage[1]

$$H = P_t + \tfrac{1}{2}\rho U_t^2 + \tfrac{1}{2}\rho(\overline{u^2}+\overline{v^2}+\overline{w^2}) \tag{2}$$

$$P = P_t + \tfrac{1}{4}\rho(\overline{v^2}+\overline{w^2}). \tag{3}$$

These expressions have been widely quoted and are probably often used for flows quite different from those for which they were suggested to hold by the original authors. It is therefore interesting to find the result of applying them to the flow under discussion in the present report.

If we further assume that the turbulence is isotropic (this is nearly true on the axis) we have

$$H = P_t + \tfrac{1}{2}\rho U_t^2 + \tfrac{3}{2}\rho\overline{v^2} \tag{2a}$$

$$P = P_t + \tfrac{1}{2}\rho\overline{v^2}. \tag{3a}$$

Using (1) we find

$$B - P_t = 2(B-P)$$

so that the true static-pressure defect is twice the measured value. We also have

$$\tfrac{1}{2}\rho U_t^2 = H_t - P_t = H - P - \rho\overline{v^2} = \tfrac{1}{2}\rho U^2 - \rho\overline{v^2}.$$

In the particular case of the measurements on the axis at $x = 28$ in. we have that $(B-P) = (H-P)/10$, and (still ignoring compressibility effects) we find

$$B - P_t = \tfrac{1}{4}(H_t - P_t)$$

$$U_t^2 = \tfrac{4}{5}U^2$$

so that the static-pressure defect is 25 per cent of the dynamic head rather than 10 per cent as 'measured'. The true velocity is 10 per cent smaller than the measured value. We note that

$$\frac{\sqrt{\overline{v^2}}}{U_t} = 0{\cdot}35.$$

If, again at $x = 28$ in., we move away from the axis the situation becomes worse. Retaining, somewhat unrealistically, the assumption of isotropy we find that the errors are steadily increasing because $(B-P)/(H-P)$ increases with r increasing reaching values of the order unity near the edge of the jet.

Our conclusion is therefore that either

(i) The study of turbulent jets by pressure measurements is highly inaccurate, or

(ii) the classical corrections to the readings of pitot and static tubes are inadequate.

The solution of the problems set by these alternatives is a matter of some urgency, and the author hopes that the present investigation may help to stimulate further research in these fields.

One or two remarks may help to throw a little more light on the problem and, at the same time, sharpen the horns of the dilemma.

Miller and Comings[4] measured $U(U_t)$ and $\overline{u^2}$ using a hot wire and P using a disc-type static-pressure probe. No corrections were applied to the static-pressure reading. Nevertheless Miller and Comings found excellent agreement between the distribution of P and the distribution of $\overline{v^2}$ as calculated from the Reynolds equations.

In the following Section 3(h) we calculate the momentum flux across a cross section of the jet as

$$R = 2\pi \int_0^\infty r\{\rho U^2 - (B-P)\}\, dr$$

and compare it with the ideal value R_i of the momentum flux at the exit assuming atmospheric pressure at the exit. Although there is some scatter it is reasonable to say that R is about 5 per cent higher than R_i.

The correct expression for the momentum integral is (*see* Ref. 6)

$$R_t = 2\pi \int_0^\infty r\rho\{U_t^2 + \overline{u^2} - \overline{v^2}\}\, dr\,.$$

Making the same assumptions as before we have that

$$\frac{R}{R_t} = 1 + \frac{3}{2}\frac{\overline{v^2}}{\overline{U_t^2}}.$$

Qualitatively we would therefore expect high values of R where the turbulence is high and we would expect a fairly pronounced maximum in the neighbourhood of $x = 28$ in. This is not apparent at all, although we do, as mentioned, find a general tendency for R to be higher than $R_i(= R_t)$.

(*h*) *Integrations Across the Mixing Region.* For each value of x from $x = 3$ in. the rate of mass flow Q, the momentum flux R, and the kinetic-energy flux K were found by numerical integration and compared with the ideal values Q_i, R_i and K_i.

The integrals are

$$Q = 2\pi \int_0^\infty r\rho U\, dr \tag{4}$$

$$R = 2\pi \int_0^\infty r\{\rho U^2 + (P-B)\}\, dr \tag{5}$$

$$K = \pi \int_0^\infty r\rho U^3\, dr\,. \tag{6}$$

In the equation for R we have included a term $(P-B)$ which must be taken into account because the calculation of R_i is based on the assumption of constant pressure equal to B in the exit plane $x = 0$.

At each value of x two values of each of the quantities Q, R and K were obtained, one from each side of the jet. Average values are shown in Fig. 28. They show a fairly large scatter. This is not surprising because of the large uncertainties in U at the outer edge of the jet where, although U is small, r is large and the contributions to the integrals therefore important.

In fully self-preserving incompressible flow we have $U \propto (x-x_0)^{-1}$ and $r_{0.5} \propto (x-x_0)$. This gives $Q \propto (x-x_0)$, R = constant, and $K \propto (x-x_0)^{-1}$. We find that the curves have roughly the

expected form. The deviations are due to the combined effects of experimental scatter, errors due to turbulence, compressibility, and lack of self-preservation. It is therefore not possible to analyse them in detail.

We note that at large values of x the rate of increase of Q is roughly Q_i per $7r_N$. It would be interesting to calculate the entrainment rates for different values of x and hence deduce the external velocity field. The only conclusion that can be reached from the Q-graph on Fig. 28 is that the entrainment per unit length is smaller close to the exit than far downstream.

4. *General Discussion and Conclusions.* An axially-symmetric jet (Jet 6) with nearly uniform initial flow of Mach number 1·40 was investigated in great detail in the region up to $x = 200r_N$. The results are discussed separately for two regions, x between 0 and $7r_N$, and x between 7 and $200r_N$.

In the first region the flow was essentially of the half-jet type and comparisons were possible with results obtained on a similar jet (Jet 1) with stronger internal disturbances and reported in Part I. It was found that there were substantial differences between the mixing regions of the two jets. Jet 6 showed a slight asymmetry not observed in Jet 1. The initial rate of spreading was larger in Jet 6 than in Jet 1 and the rate of spreading was almost constant over the whole of the first region at a value only slightly smaller than that found in low-speed flow. In Jet 1 the initial rate of spreading was found to be only about half the low-speed value, and there was a sudden change over to the low-speed value at $x = 2 \cdot 7r_N$. No satisfactory explanation was found for this difference between the two jets. The velocity profiles in the first region of Jet 6 were found to be similar and well approximated by an error-function profile.

In the second region of Jet 6 the central core disappeared rapidly and the velocity profiles quickly became similar. They were reasonably well represented by a Gaussian profile. Fully self-preserving flow with linear rate of spreading was, however, only approached very slowly and the static-pressure profiles demonstrated that self-preservation was not reached even at $x = 200r_N$.

The static-pressure profiles indicated large variations in the turbulence intensity with a maximum at about $75r_N$. In regions of high turbulence it was found that if the classical corrections to the readings of pitot and static tubes are adequate, the measurements in the jet are highly inaccurate.

Integrations across the jet showed the expected variations with x of the rate of mass flow, the momentum flux, and the kinetic-energy flux.

The investigations reported in the present paper together with the results given in Part I demonstrate that there are a number of problems in connection with jet flows which are not fully understood and require further investigations. In particular, it must be concluded that further work based entirely on pressure measurements, although they may give results of value for practical engineering problems, are unlikely to lead to a full understanding of the phenomena involved in jet flows. Turbulence measurements are urgently needed, and it is the author's opinion that a re-examination of the classical expressions for the corrections to the readings of pitot and static tubes in turbulent flow is overdue.

The very slow approach to self-preservation was already pointed out by Townsend[6]. In fact, the results presented in the present paper suggest that full self-preservation may never in practice be reached at measurable velocities. Put another way, it may not be reached until the velocities are so low that they are of the same order as the random velocity fluctuations in the 'still' air into which the jet is issuing.

NOTATION

B	Barometric pressure
F_1, F_2	Functions defined in Section 4(c) of Part I
F_3	Function defined in Section 3(d)
H	Pitot pressure
K	Kinetic-energy flux
P	Static pressure
Q	Rate of mass flow
R	Momentum flux
U	Velocity
r	Radius (distance from axis of jet)
u, v, w	Turbulent-velocity components in cylindrical co-ordinates (x, r, θ)
x	Distance from nozzle exit
x_0	Virtual origin
x'	Distance from virtual origin
y	Distance across jet
y'	Distance from point where $U/U_1 = 0{\cdot}5$
ρ	Density
σ	Scale factor {equation (3) of Part I}

Suffices

N	Nozzle exit
i	Ideal values
t	True values {used in Section 3 (g) only}
$0{\cdot}5$	Values at $U/U_1 = 0{\cdot}5$
1	Values at inner edge of mixing region or on axis of jet

REFERENCES

No.	*Author*	*Title, etc.*
1	A. Fage	On the static pressure in fully developed turbulent flow. *Proc. Roy. Soc.* A. Vol. 155. p.576. 1936.
2	S. Goldstein	A note on the measurement of total head and static pressure in a turbulent stream. *Proc. Roy. Soc.* A. Vol. 155. p.570. 1936.
3	N. H. Johannesen	The mixing of free axially-symmetrical jets of Mach number 1·40. A.R.C. R. & M. 3291. January, 1957.
4	D. R. Miller and E. W. Comings ..	Static pressure distribution in the free turbulent jet. *J. Fluid Mech.* Vol. 3. p.1. 1957.
5	E. T. Pitkin and I. Glassman ..	Experimental mixing profiles of a Mach 2·6 free jet. *J. Aero/Space Sci.* Vol. 25. p.791. 1958.
6	A. A. Townsend	*The structure of turbulent shear flow.* Cambridge University Press. 1956.
7	W. R. Warren	The static pressure variation in compressible free jets. *J. Ae. Sci.* Vol. 22. p.205. 1955.

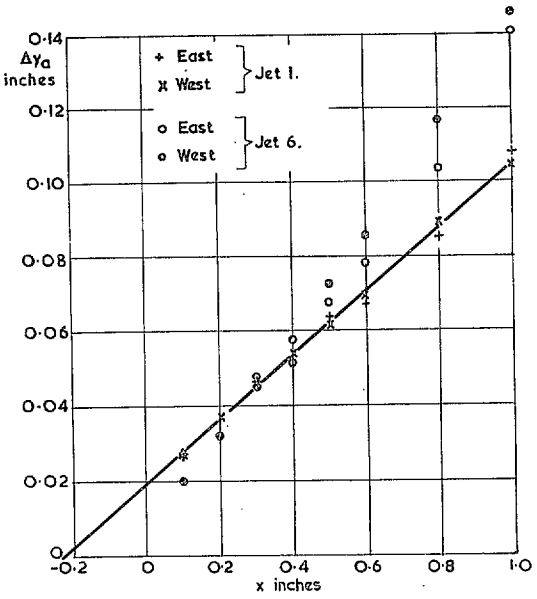

FIG. 1. Δy_a for $0{\cdot}1$ in. $\leqslant x \leqslant 1{\cdot}0$ in.

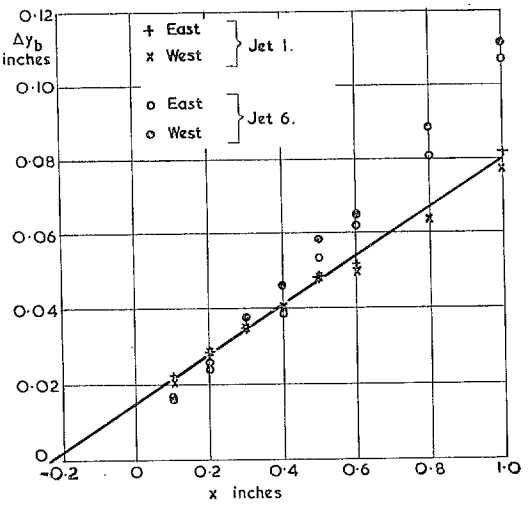

FIG. 2. Δy_b for $0{\cdot}1$ in. $\leqslant x \leqslant 1{\cdot}0$ in.

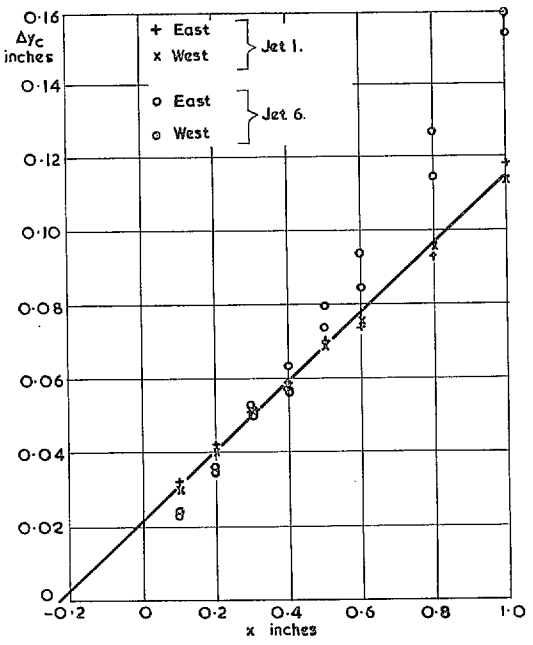

FIG. 3. Δy_c for $0{\cdot}1$ in. $\leqslant x \leqslant 1{\cdot}0$ in.

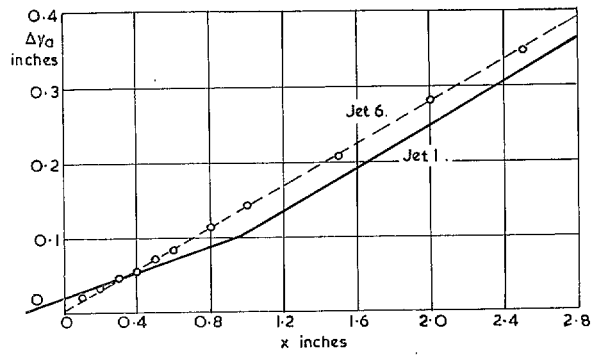

FIG. 4. Δy_a for $0{\cdot}1$ in. $\leqslant x \leqslant 2{\cdot}5$ in.

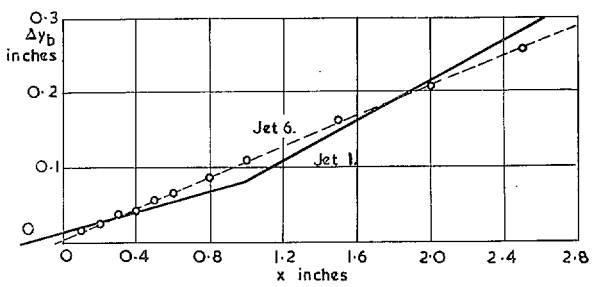

FIG. 5. Δy_b for $0{\cdot}1$in. $\leqslant x \leqslant 2{\cdot}5$ in.

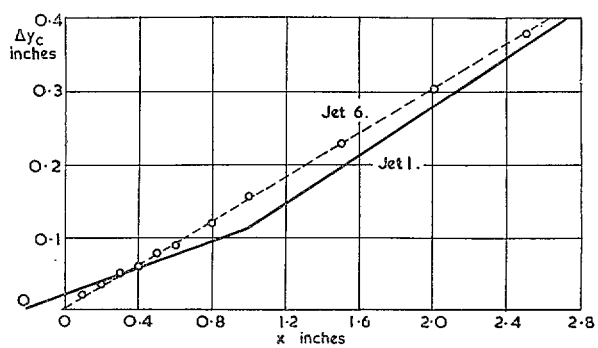

FIG. 6. Δy_c for $0{\cdot}1$ in. $\leqslant x \leqslant 2{\cdot}5$ in.

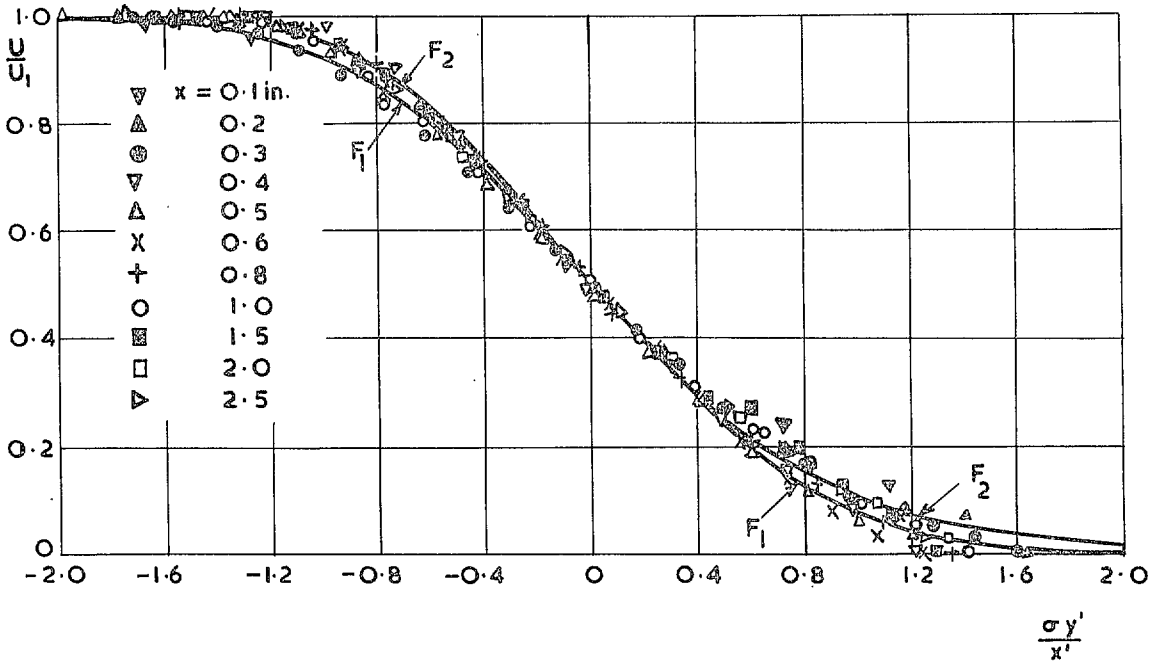

FIG. 7. Similarity of velocity profiles. Jet 6 East $\sigma = 13{\cdot}7$.

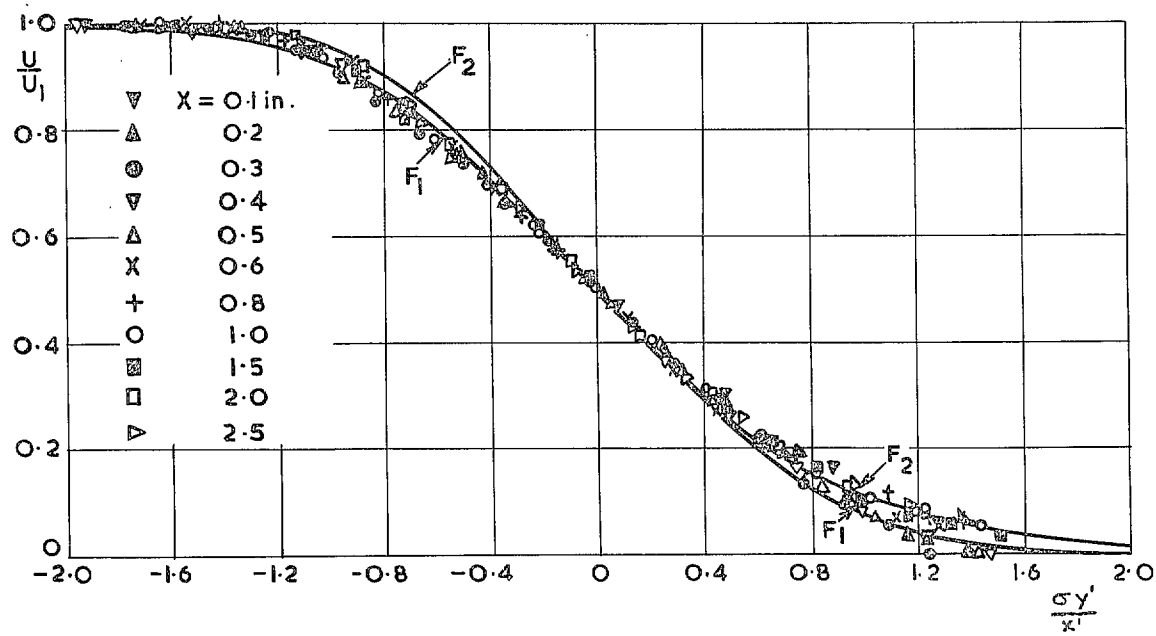

FIG. 8. Similarity of velocity profiles. Jet 6 West $\sigma = 13{\cdot}7$.

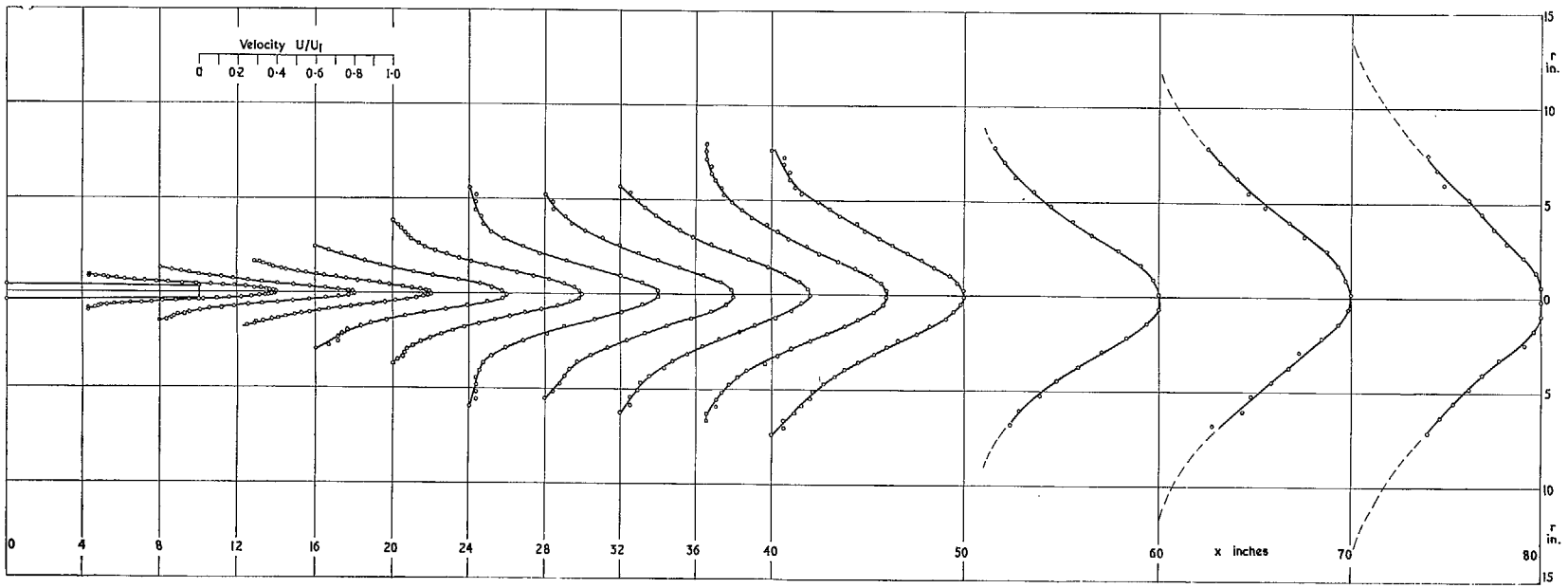

FIG. 9. Velocity profiles. Jet 6.

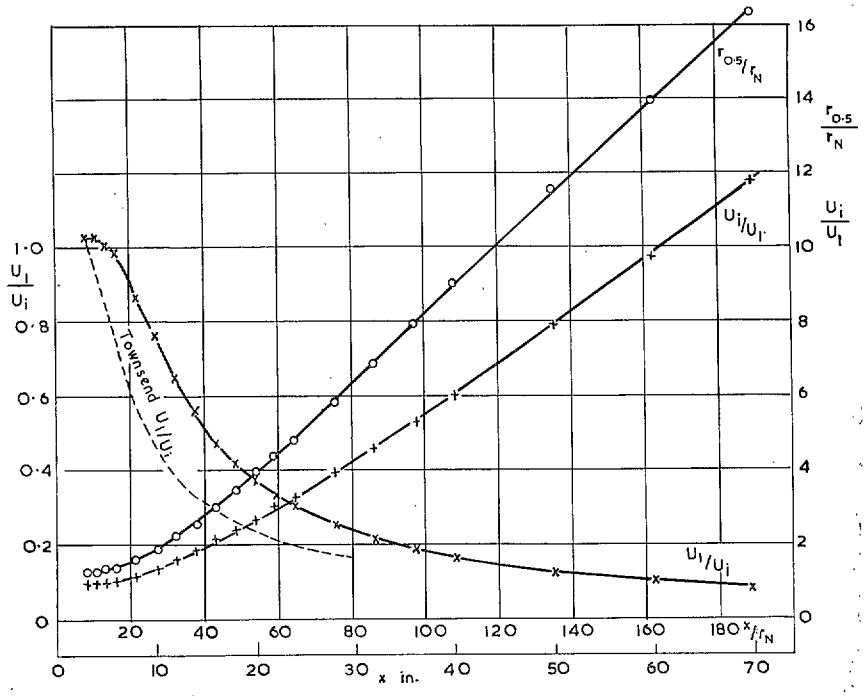

FIG. 10. Axial velocity and jet width.

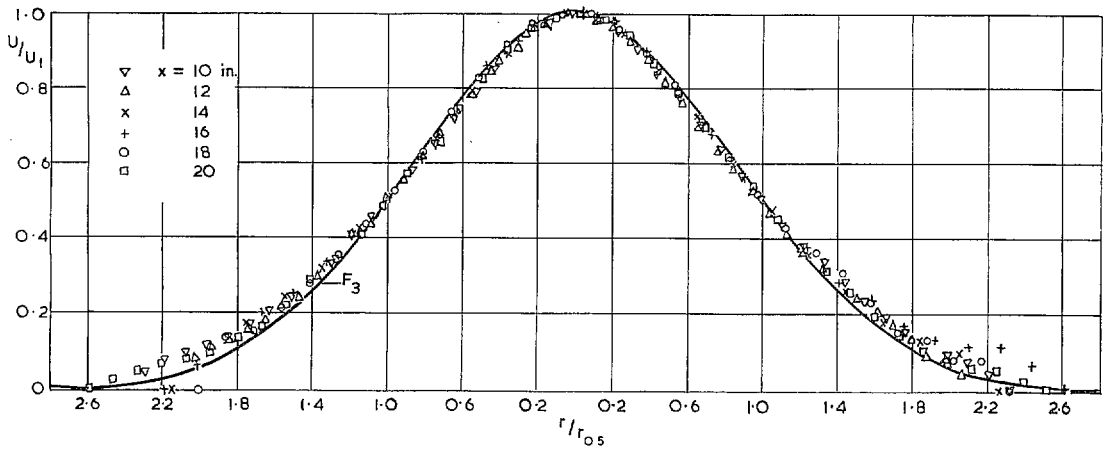

FIG. 11. Similarity of velocity profiles. Jet 6.

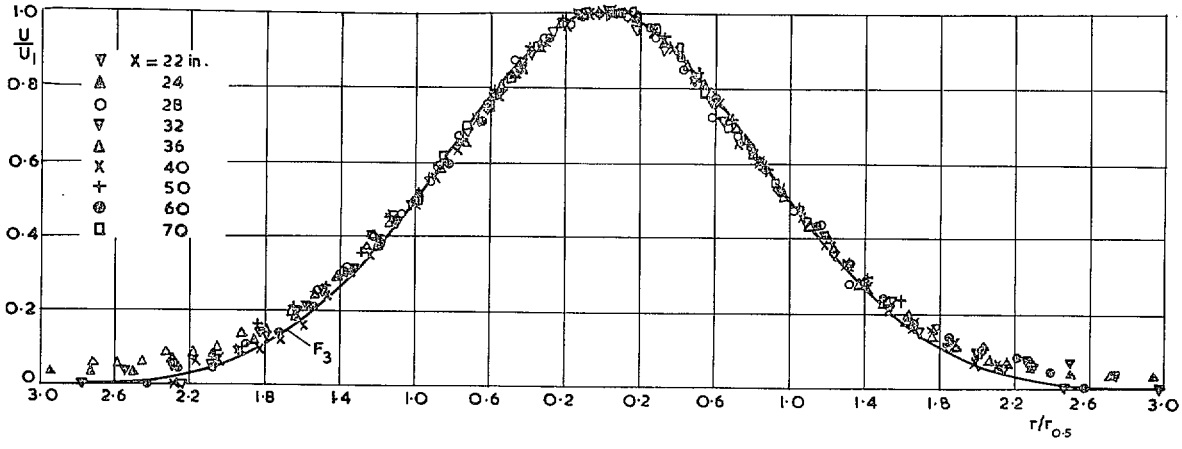

FIG. 12. Similarity of velocity profiles. Jet 6.

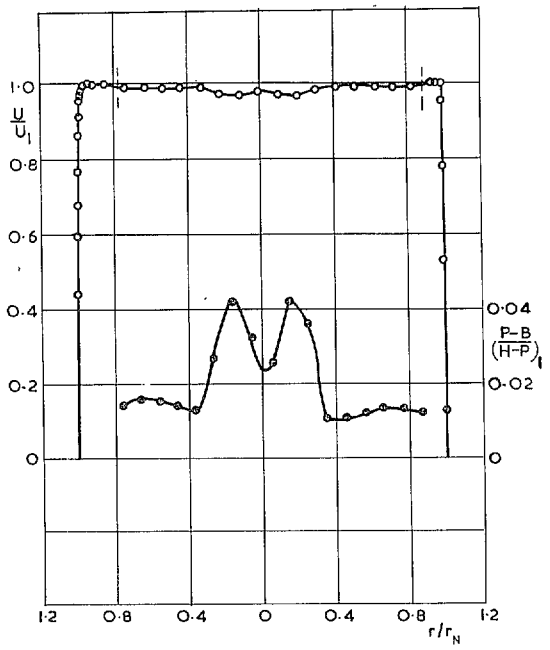

FIG. 13. Velocity and pressure distributions. Jet 6. $x = 0{\cdot}0$ in.

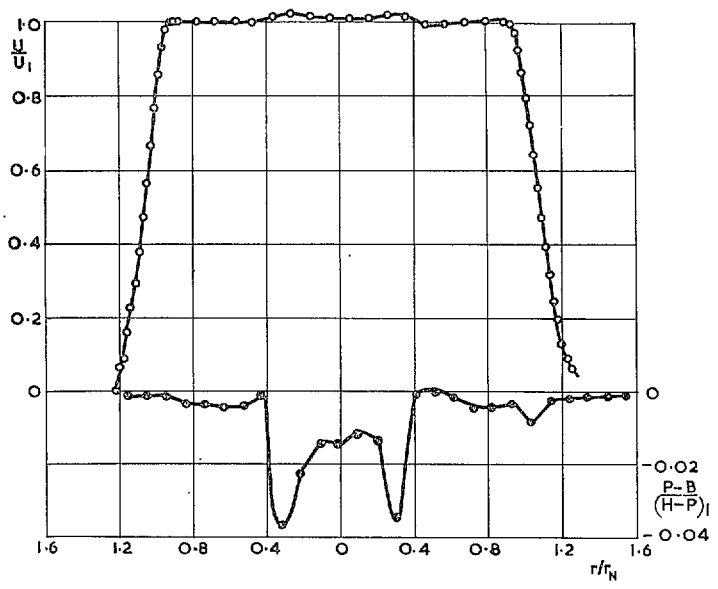

FIG. 14. Velocity and pressure distributions. Jet 6. $x = 0{\cdot}6$ in.

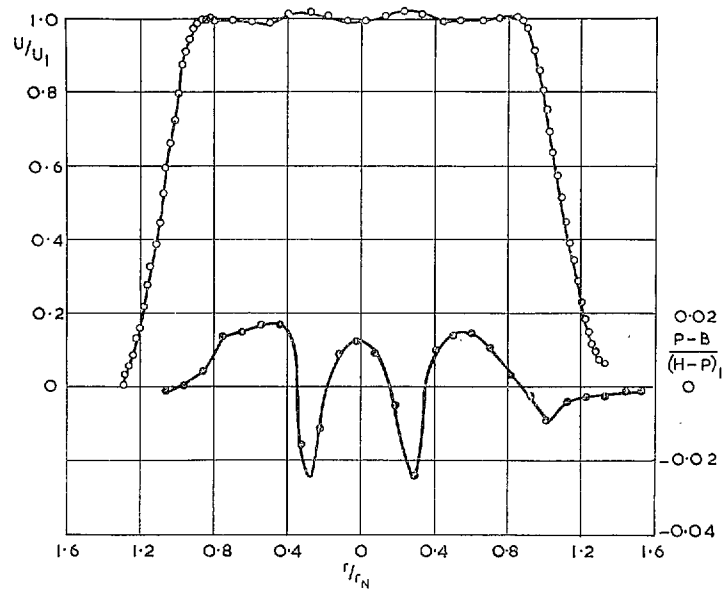

FIG. 15. Velocity and pressure distributions. Jet 6.
$x = 0 \cdot 8$ in.

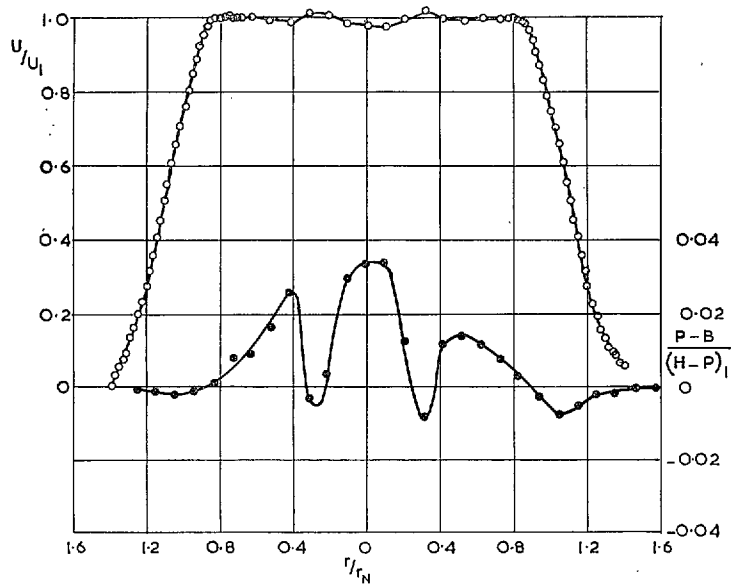

FIG. 16. Velocity and pressure distributions. Jet 6.
$x = 1 \cdot 0$ in.

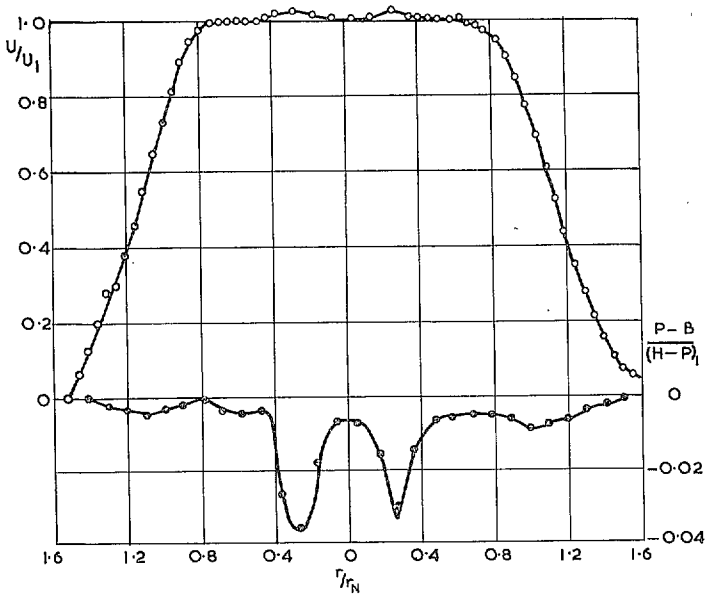

FIG. 17. Velocity and pressure distributions. Jet 6. $x = 1{\cdot}5$ in.

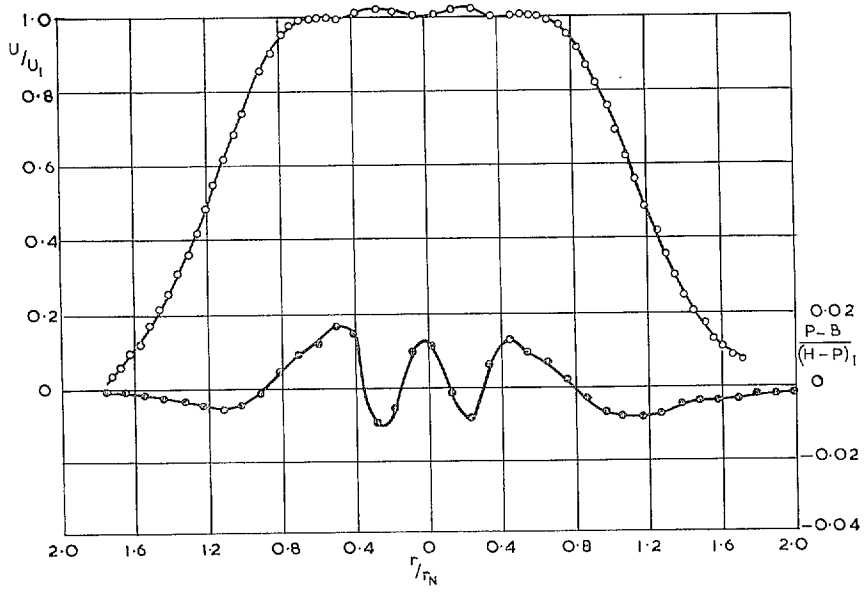

FIG. 18. Velocity and pressure distributions. Jet 6. $x = 2{\cdot}0$ in.

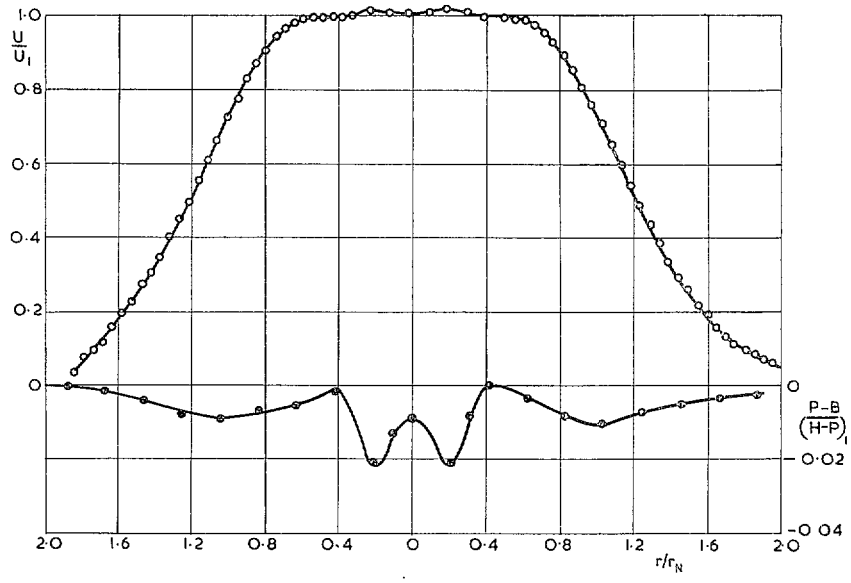

FIG. 19. Velocity and pressure distributions. Jet 6. $x = 2{\cdot}5$ in.

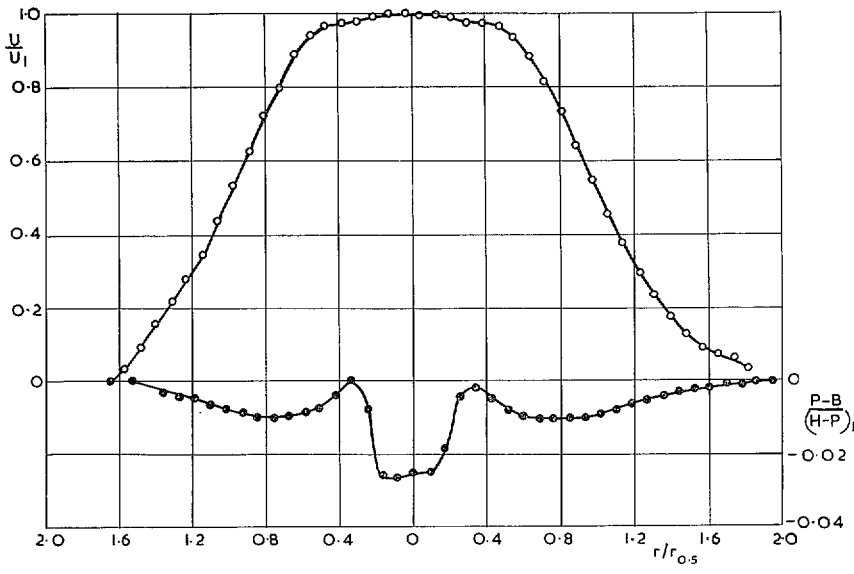

FIG. 20. Velocity and pressure distributions. Jet 6. $x = 3{\cdot}0$ in.

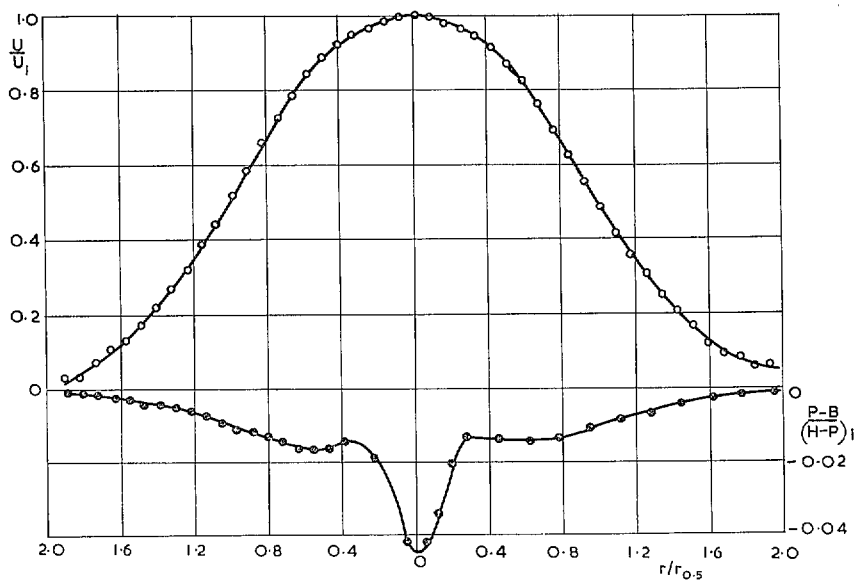

FIG. 21. Velocity and pressure distributions. Jet 6. $x = 4{\cdot}0$ in.

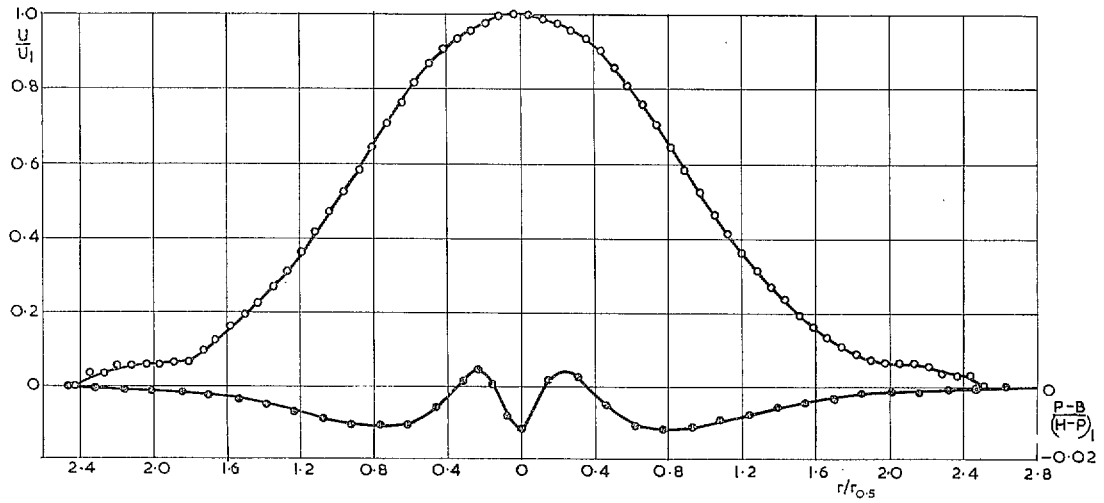

FIG. 22. Velocity and pressure distributions. Jet 6. $x = 5{\cdot}0$ in.

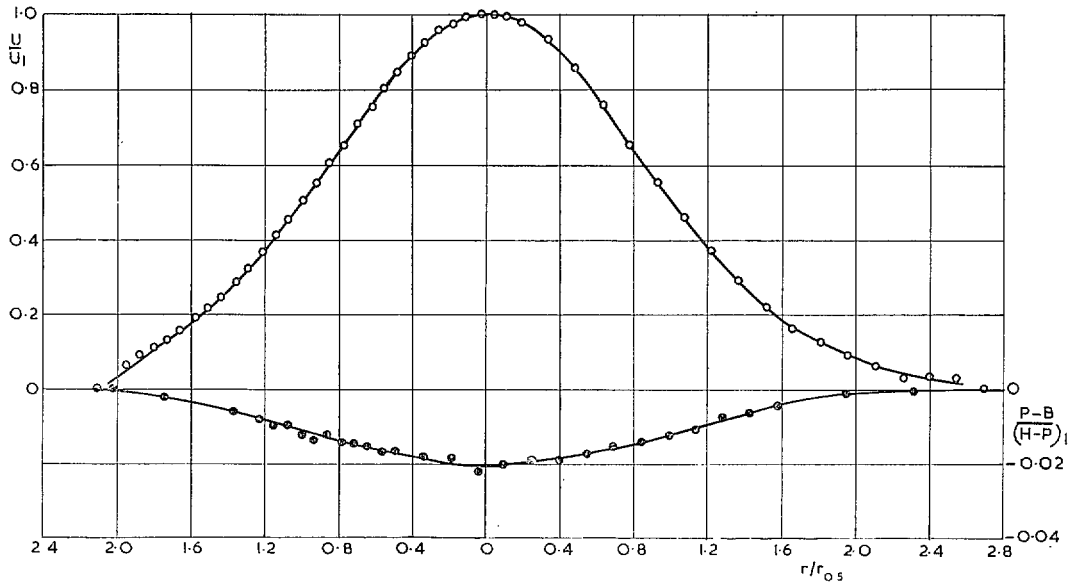

FIG. 23. Velocity and pressure profiles. Jet 6. $x = 6 \cdot 0$ in.

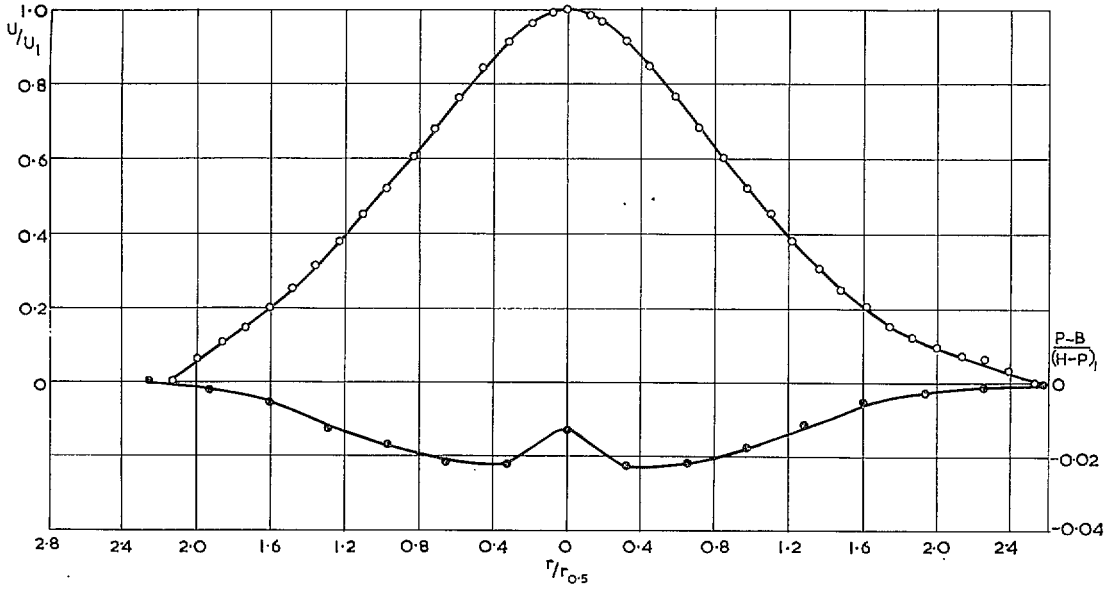

FIG. 24. Velocity and pressure profiles. Jet 6. $x = 8 \cdot 0$ in.

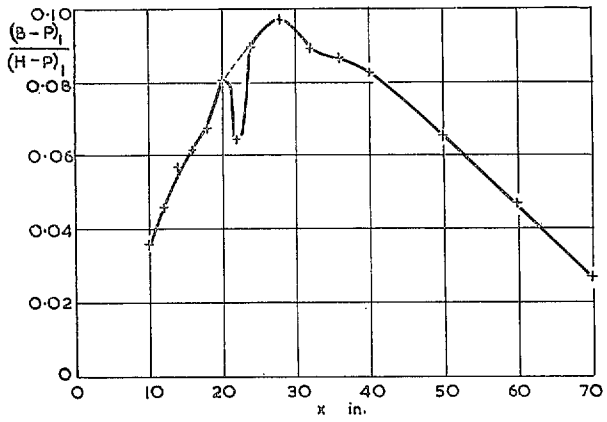

FIG. 25. Static pressure on axis. Jet 6.

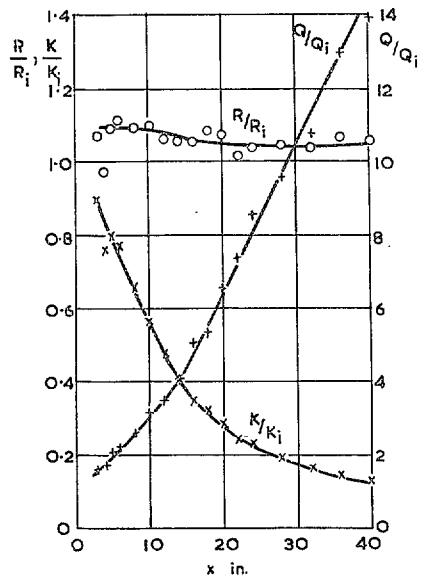

FIG. 28. Integrated values of Q, R, K.

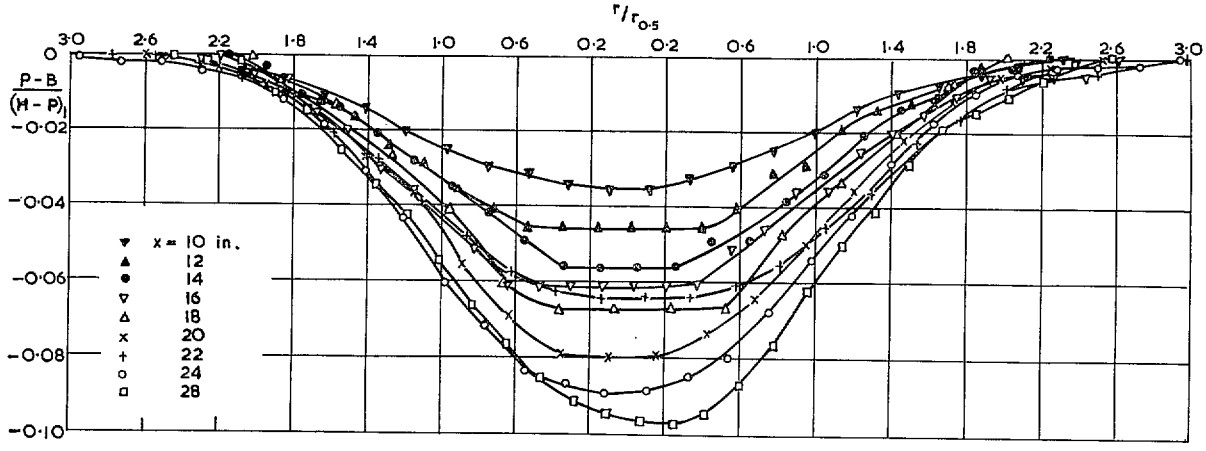

FIG. 26. Pressure distributions. Jet 6.

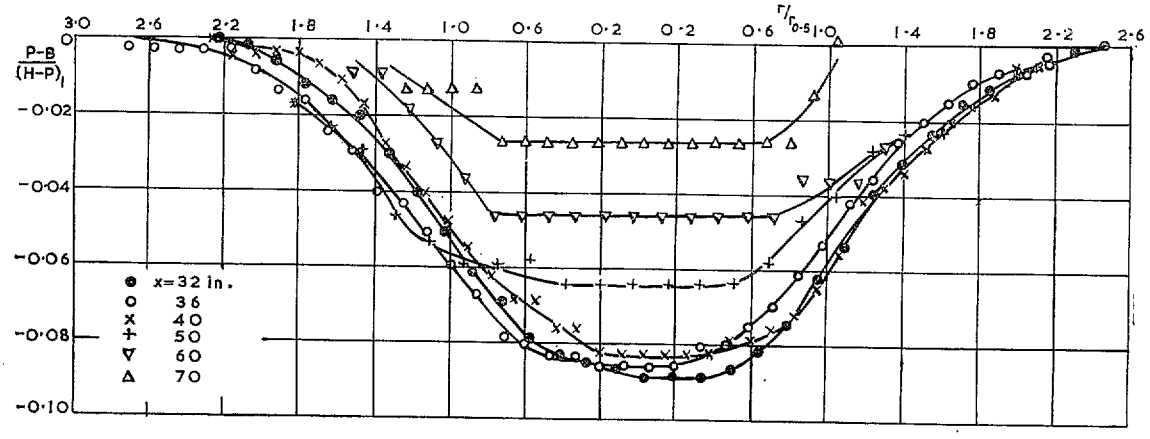

FIG. 27. Pressure distributions. Jet 6.

(85436) Wt. 64/1857 K.5 12/62 Hw.

Publications of the Aeronautical Research Council

ANNUAL TECHNICAL REPORTS OF THE AERONAUTICAL RESEARCH COUNCIL (BOUND VOLUMES)

1942 Vol. I. Aero and Hydrodynamics, Aerofoils, Airscrews, Engines. 75*s.* (post 2*s.* 9*d.*)
Vol. II. Noise, Parachutes, Stability and Control, Structures, Vibration, Wind Tunnels. 47*s.* 6*d.* (post 2*s.* 3*d.*)

1943 Vol. I. Aerodynamics, Aerofoils, Airscrews. 80*s.* (post 2*s.* 6*d.*)
Vol. II. Engines, Flutter, Materials, Parachutes, Performance, Stability and Control, Structures. 90*s.* (post 2*s.* 9*d.*)

1944 Vol. I. Aero and Hydrodynamics, Aerofoils, Aircraft, Airscrews, Controls. 84*s.* (post 3*s.*)
Vol. II. Flutter and Vibration, Materials, Miscellaneous, Navigation, Parachutes, Performance, Plates and Panels, Stability, Structures, Test Equipment, Wind Tunnels. 84*s.* (post 3*s.*)

1945 Vol. I. Aero and Hydrodynamics, Aerofoils. 130*s.* (post 3*s.* 6*d.*)
Vol. II. Aircraft, Airscrews, Controls. 130*s.* (post 3*s.* 6*d.*)
Vol. III. Flutter and Vibration, Instruments, Miscellaneous, Parachutes, Plates and Panels, Propulsion. 130*s.* (post 3*s.* 3*d.*)
Vol. IV. Stability, Structures, Wind Tunnels, Wind Tunnel Technique. 130*s.* (post 3*s.* 3*d.*)

1946 Vol. I. Accidents, Aerodynamics, Aerofoils and Hydrofoils. 168*s.* (post 3*s.* 9*d.*)
Vol. II. Airscrews, Cabin Cooling, Chemical Hazards, Controls, Flames, Flutter, Helicopters, Instruments and Instrumentation, Interference, Jets, Miscellaneous, Parachutes. 168*s.* (post 3*s.* 3*d.*)
Vol. III. Performance, Propulsion, Seaplanes, Stability, Structures, Wind Tunnels. 168*s.* (post 3*s.* 6*d.*)

1947 Vol. I. Aerodynamics, Aerofoils, Aircraft. 168*s.* (post 3*s.* 9*d.*)
Vol. II. Airscrews and Rotors, Controls, Flutter, Materials, Miscellaneous, Parachutes, Propulsion, Seaplanes, Stability, Structures, Take-off and Landing. 168*s.* (post 3*s.* 9*d.*)

1948 Vol. I. Aerodynamics, Aerofoils, Aircraft, Airscrews, Controls, Flutter and Vibration, Helicopters, Instruments, Propulsion, Seaplane, Stability, Structures, Wind Tunnels. 130*s.* (post 3*s.* 3*d.*)
Vol. II. Aerodynamics, Aerofoils, Aircraft, Airscrews, Controls, Flutter and Vibration, Helicopters, Instruments, Propulsion, Seaplane, Stability, Structures, Wind Tunnels. 110*s.* (post 3*s.* 3*d.*)

Special Volumes

Vol. I. Aero and Hydrodynamics, Aerofoils, Controls, Flutter, Kites, Parachutes, Performance, Propulsion, Stability. 126*s.* (post 3*s.*)
Vol. II. Aero and Hydrodynamics, Aerofoils, Airscrews, Controls, Flutter, Materials, Miscellaneous, Parachutes, Propulsion, Stability, Structures. 147*s.* (post 3*s.*)
Vol. III. Aero and Hydrodynamics, Aerofoils, Airscrews, Controls, Flutter, Kites, Miscellaneous, Parachutes, Propulsion, Seaplanes, Stability, Structures, Test Equipment. 189*s.* (post 3*s.* 9*d.*)

Reviews of the Aeronautical Research Council

1939–48 3*s.* (post 6*d.*) 1949–54 5*s.* (post 5*d.*)

Index to all Reports and Memoranda published in the Annual Technical Reports

1909–1947 R. & M. 2600 (out of print)

Indexes to the Reports and Memoranda of the Aeronautical Research Council

Between Nos. 2351–2449	R. & M. No. 2450 2*s.* (post 3*d.*)
Between Nos. 2451–2549	R. & M. No. 2550 2*s.* 6*d.* (post 3*d.*)
Between Nos. 2551–2649	R. & M. No. 2650 2*s.* 6*d.* (post 3*d.*)
Between Nos. 2651–2749	R. & M. No. 2750 2*s.* 6*d.* (post 3*d.*)
Between Nos. 2751–2849	R. & M. No. 2850 2*s.* 6*d.* (post 3*d.*)
Between Nos. 2851–2949	R. & M. No. 2950 3*s.* (post 3*d.*)
Between Nos. 2951–3049	R. & M. No. 3050 3*s.* 6*d.* (post 3*d.*)
Between Nos. 3051–3149	R. & M. No. 3150 3*s.* 6*d.* (post 3*d.*)

HER MAJESTY'S STATIONERY OFFICE

from the addresses overleaf

Printed and published by
HER MAJESTY'S STATIONERY OFFICE

To be purchased from
York House, Kingsway, London W.C.2
423 Oxford Street, London W.1
13A Castle Street, Edinburgh 2
109 St. Mary Street, Cardiff
39 King Street, Manchester 2
50 Fairfax Street, Bristol 1
35 Smallbrook, Ringway, Birmingham 5
80 Chichester Street, Belfast 1
or through any bookseller

Printed in England

S.O. Code No. 23-3292